Journal of Alloys and Compounds 504 (2010) 141–145

Contents lists available at ScienceDirect

Journal of Alloys and Compounds

journal homepage: www.elsevier.com/locate/jallcom

Preparation and characterization of Mg-doped fluorapatite nanopowders by sol–gel method

M. Kheradmandfard*, M.H. Fathi

Biomaterials Group, Department of Materials Engineering, Isfahan University of Technology, Isfahan, 84156-83111, Iran

ARTICLE INFO

Article history:
Received 20 December 2009
Received in revised form 14 May 2010
Accepted 21 May 2010
Available online 1 June 2010

Keywords:
Ceramics
Nanostructured materials
Sol–gel processes
X-ray diffraction

ABSTRACT

Properties of hydroxyapatite (HA) or fluorapatite (FA), such as bioactivity, biocompatibility, solubility, and adsorption properties can be tailored over a wide range by modifying the composition via ionic substitutions. This research aimed to prepare and characterize Mg-doped FA (Mg-FA) nanopowders. Mg-FA nanopowders with different Mg contents were prepared by sol–gel method. The designated degree of substitution of Ca^{2+} by Mg^{2+} in the mixture was determined by the x value in the general formula of ($Ca_{10-x}Mg_x(PO_4)_6F_2$), where $x = 0$, 0.25, 0.5, 0.75, and 1. X-ray diffraction (XRD), scanning electron microscopic (SEM), transmission electron microscopy (TEM), atomic absorption spectrophotometer (AAS) and Fourier transform infrared spectroscopy (FTIR) techniques were utilized to characterize the obtained powders. Results showed that Mg ions entered into the fluorapatite lattice and occupied Ca^{2+} sites. The incorporation of Mg ions into the fluorapatite resulted in the decrease of the lattice parameters. The obtained powders had crystallite size of about 30–100 nm.

1. Introduction

Hydroxyapatite ($Ca_{10}(PO_4)_6(OH)_2$, HA) has been widely used for biomedical applications due to its bioactive, biocompatible and osteoconductive properties [1–4]. Despite these desirable properties, synthetic HA is limited in application due to poor thermostability, high in vivo solubility and poor mechanical properties [5–7]. Various amounts of substitutions (i.e. F^-, $CO3^{2-}$, Na^+, Mg^{+2}, Zn^{+2}) are present in biological apatites [8]. Properties of HA, such as bioactivity, biocompatibility, solubility, and adsorption properties can be tailored over a wide range by modifying the composition via ionic substitutions [9,10].

Fluorine-substituted HA ($Ca_{10}(PO_4)_6(OH)_xF_{2-x}$, FHA) and fluorapatite ($Ca_{10}(PO_4)_6F_2$, FA), in which the hydroxylic groups (OH^-) are substituted by F^- ions, are considered as alternative biomedical materials and have the potential for use in dental implants [11–13]. The introduction of fluoride into apatite has been shown to be beneficial factor in improving osteoblast response in terms of adhesion, differentiation, proliferation and mineralization processes, compared to pure hydroxyapatite [14]. Fluorine replacement reduces the solubility, stimulates the formation of bone tissue, and increases the compression strength [15].

Mg is one of the most important substitutes for calcium in biological apatites. Dentin, Enamel, and bone contain 1.23, 0.44 and 0.72 wt% of Mg, respectively [9]. Mg is strongly associated with the mineralization of calcified tissues, directly stimulating osteoblast proliferation [16]. The adhesion strength between substrate and apatite coating is increased as magnesium is incorporated into the apatite coating [17]. Liang et al. [18] found that Mg implantation improves the bioactivity of zirconia and titanium. The presence of Mg in the FHA coating significantly affects the bone growth (formation of new apatite layer) in SBF, i.e. the in vitro bioactivity of the coating [19]. The sol–gel technique, because of its apparent advantages of fine homogeneity, high reactivity of starting materials, lower processing temperature and lower sintering temperature, is a new method for synthesizing fine powders. Moreover, this method permits researchers to easily dope HA or FA with trace elements [20–22].

Considering the above points in view, Mg-FA materials may then be superior to pure FA for implant applications.

In this work, we prepared Mg-FA powders in order to integrate the advantages of Mg with the low soluble ability of FA. The powders with different Mg contents were prepared by sol–gel method, and the effects of Mg incorporation on the powders were investigated.

2. Experimental

2.1. Powder preparation

The flowchart of the preparation method of Mg-FA nanopowder in this study is shown in Fig. 1. Calcium nitrate tetrahydrate ($Ca(NO_3)_2{\cdot}4H_2O$; Merck), magnesium nitrate hexahydrate ($Mg(NO_3)_2{\cdot}6H_2O$; Merck), phosphorus pentoxide (P_2O_5; Merck) and hexafluorophosphoric acid (HPF6; Floka) were selected to prepare Ca-

* Corresponding author. Tel.: +98 311 3912750; fax: +98 311 3912752.
E-mail address: mkh_fard@yahoo.com (M. Kheradmandfard).

0925-8388/$ – see front matter © 2010 Elsevier B.V. All rights reserved.
doi:10.1016/j.jallcom.2010.05.073

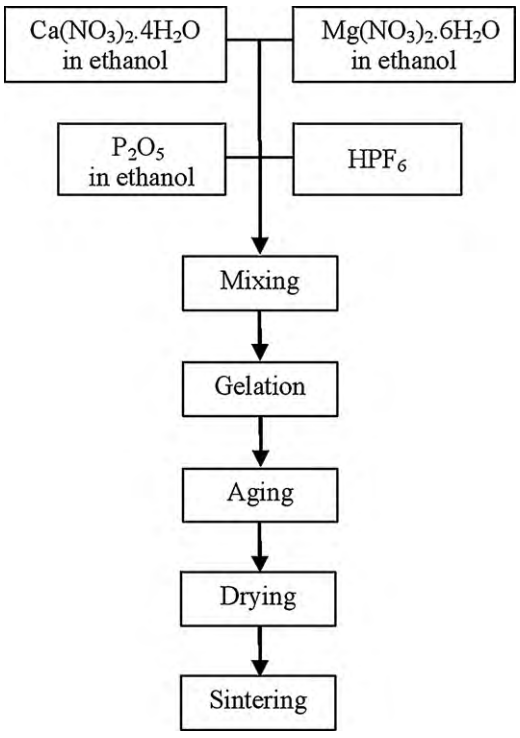

Fig. 1. Flowchart of the sol–gel synthesis of Mg-FA nanopowder.

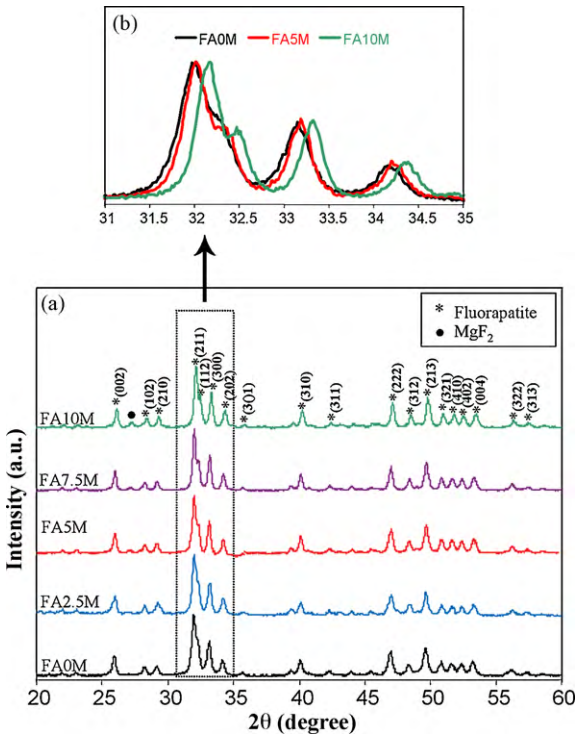

Fig. 2. XRD patterns of Mg-FA nanopowders calcined at 650 °C.

precursor, Mg-precursor, P-precursor and F-precursor, respectively. A designated amount of phosphoric pentoxide (P_2O_5, Merck) was dissolved in absolute ethanol. Also, a designated amount of Mg-precursor and Ca-precursor was mixed to form the Ca–Mg mixture and then dissolved in absolute ethanol. This mixture was added drop-wise into the P-precursor to obtain a solution with (Ca, Mg)/P ratio of 1.67. Then, HPF_6 was added to the solution. The designated degree of substitution of Ca^{2+} by Mg^{2+} in the mixture was determined by the x value in the general formula of FA ($Ca_{10-x}Mg_x(PO_4)_6F_2$), where x = 0, 0.25, 0.5, 0.75 and 0.1. The subsequent powders were labeled as FA0M, FA2.5M, FA5M, FA7.5M and FA10M, respectively. The mixture was continuously stirred for about 24 h at ambient temperature to form a gel. As-formed gel was aged for 24 h, and then it was dried in an oven at 100 °C in air for 24 h. The dried gel was sintered at a rate of 5 °C/min up to 650 °C for 1 h in a muffle furnace.

2.2. Powder characterization

Phase structure analyses were carried out by X-ray diffraction (XRD) using a Philips X'Pert-MPD diffractometer with Cu Kα radiation (λ = 0.15418 nm) over the 2θ range of 20–60° (time per step: 1 s and step size: 0.02°).The obtained experimental patterns were compared to the standards compiled by the Joint Committee on Powder Diffraction and Standards (JCDPS), which involved card # 15-0876 for FA. The crystallite size of the FA nanopowders was determined by using the Scherrer equation [23]:

$$\beta = \frac{k\lambda}{t\cos\theta} \quad (1)$$

Table 1
Lattice parameters and crystallite size of the obtained powders.

Sample	a-axis (nm)	c-axis (nm)	Crystallite size (nm)
FA0M	0.93427	0.68663	29
FA2.5M	0.93408	0.68546	26
FA5M	0.93401	0.68507	34
FA7.5M	0.93401	0.68507	37
FA10M	0.92943	0.68199	37

where β is the width of peak in the middle of its height, λ is the wavelength (=0.154 nm), θ is the Bragg angle, k is a constant (=0.9), and t is the apparent crystallite size. For this purpose, three diffraction peaks (0 0 2), (2 0 2), and (2 2 2), which have the advantage of being well separated and having high intensities, were chosen for the measurement. The half-widths were calculated by sigma plot software.

Lattice parameters (c and a) were calculated from peaks (0 0 2) and (2 1 1), respectively, using the standard HCP unit cell plane spacing relationship [24]:

$$\frac{1}{d^2} = \frac{4}{3}\left(\frac{h^2+hk+k^2}{a^2}\right) + \frac{l^2}{c^2} \quad (2)$$

where d is the distance between adjacent planes in the set of Miller indices ($h\,k\,l$).

The functional groups of samples were analyzed with Fourier transform infrared (FTIR, Bomem, MB100) in a mid-IR spectrum range in the range of 400–4000 cm^{-1}. For this purpose, each powder was mixed with KBr. Mg contents were determined using an atomic absorption spectrophotometer, (AAS) (3030). The morphology and

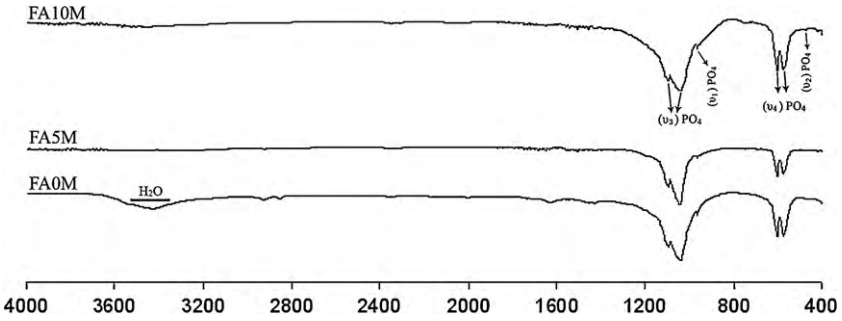

Fig. 3. FTIR spectra of sintered FA powder with different Mg contents.

agglomerates size distributions of the prepared powders were investigated by scanning electron microscopy, SEM (Phillips XL 30: Eindhoven, The Netherlands). The morphology and particle size of the powders were checked using transmission electron microscopy (TEM) working at 200 kV.

3. Results and discussion

3.1. Phase structure analysis

Fig. 2a shows the XRD patterns of Mg-FA powders which were sintered at 650 °C. FA diffraction peaks were observed for all the samples according to standard card of FA (JCDP#15-0876). It was found that the position of FA peaks shifted slightly to higher angles with increasing the Mg content of FA powders as shown in Fig. 2b. This suggests that the lattice parameters of FA reduce as a result of the substitution of Ca^{2+} with Mg ions in the FA lattice. On the other hand, since Mg ionic radius (0.065 nm) is smaller than that of Ca^{2+} ions (0.099 nm) [25], the substitution of calcium by smaller Mg ions resulted in a contraction of the cell parameters of FA. The contraction of the cell parameters of FA as a result of increasing Mg content has also been reported by Hidouri et al. [26]. Similar result has also been reached in the case of HA-containing Mg ions [25]. The lattice parameters of powders are listed in Table 1.

As can be seen (Fig. 2a), with increasing the Mg content, one small extra peak of MgF_2 phase appears on XRD patterns, suggesting that the whole Mg cannot be incorporated in FA lattice. Also, with increasing Mg content of FA powders, the intensity of MgF_2 peak increased. The appearance of extra phase on XRD patterns of Mg-FA powders is also reported by Hidouri et al. [26]. They reported that with increasing Mg content of FA powders, the $Mg_2F(PO_4)$ phase was detected. In contrast, this study led to the appearance of MgF_2.

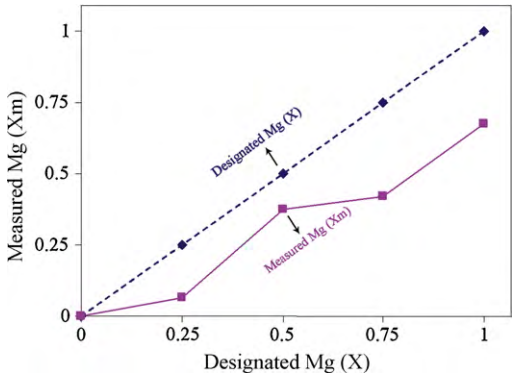

Fig. 4. Mg concentrations determined by the x value in the general formula of $(Ca_{10-x}Mg_x(PO_4)_6F_2)$ in the powders: broken line: designated: solid line: measured Mg concentrations in the powders.

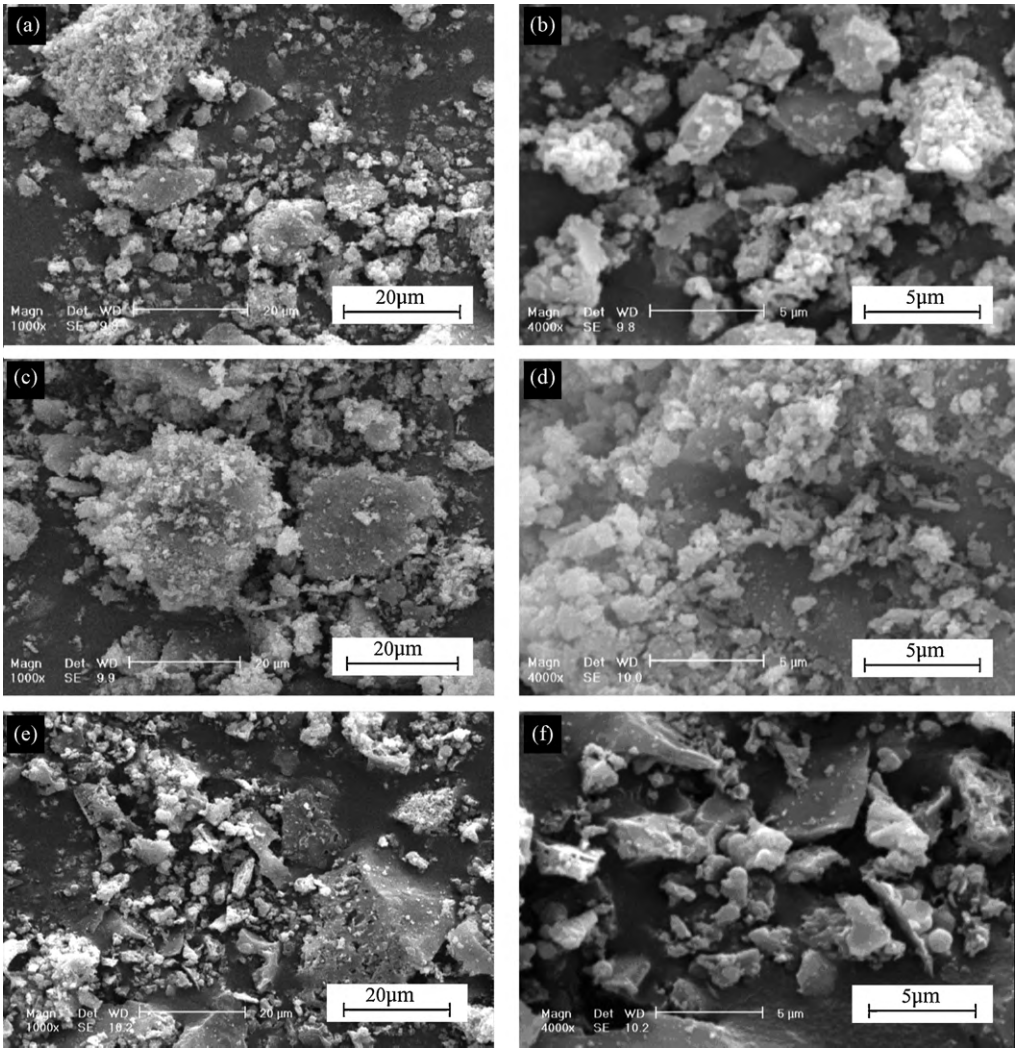

Fig. 5. SEM micrographs of (a, b) FA0M, (c, d) FA5M and (e, f) FA10M calcined powder at 650 °C.

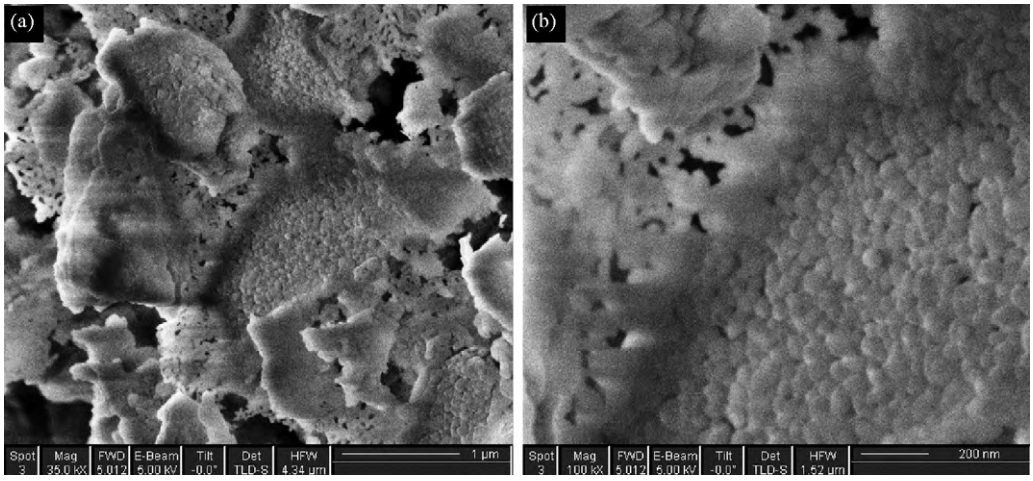

Fig. 6. SEM micrographs of FA5M powder in high magnifications.

Crystallite sizes of the prepared FA with different degrees of Mg content, calculated using XRD data, are shown in Table 1. The crystallite size of the obtained powders is in the range of 26–37 nm.

3.2. FTIR evaluation

FTIR spectra of the obtained FA powders with different Mg contents are shown in Fig. 3. The IR spectra of each of the prepared powders are characteristics of FA [26,27]. The bands at 966 and at 474 cm^{-1} were attributed to υ_1 and υ_2 vibration peaks, respectively [25,28]. The absorption peaks located at 1096 and 1045 cm^{-1} were derived from the asymmetrical stretching (υ_3) of PO_4^{3-}, and at 577 and 603 cm^{-1} they were assigned to the bending modes (υ_4) of PO_4^{3-}, respectively [25]. The bands located at 1632 and 3436 cm^{-1} in IR spectra of FA0M powder were attributed to the water present in the samples and/or absorbed in the KBr pellet [26].

3.3. Chemical analysis

Chemical analysis of the Mg-FA powders is shown in Fig. 4, where x and x_m are designated and measured Mg concentration, respectively. As can be seen, with increasing x, Mg concentration increased. In addition, x_m was smaller than x, suggesting that the Mg was partially incorporated into the FA lattice [26]. In other words, partial amount of Mg in the starting solution entered into the FA lattice. Similar results were obtained for HA [24,25,29,30], which show partial substitution of Ca with Mg in the HA lattice.

3.4. SEM analysis

Fig. 5 shows the microstructure and morphology of FA powder samples with different Mg contents. The morphology of the powders indicates that it is composed of agglomerates with wide particle size distributions. As can be seen, these samples are formed by particles of very irregular shape and dimensions, independently of Mg content. The SEM photomicrographs of FA5M powder in higher magnifications are shown in Fig. 6. As shown in Fig. 6, the agglomerated particles in Fig. 5 are composed of very fine particles.

3.5. TEM analysis

The morphological shape and size of FA5M powder obtained from TEM are shown in Fig. 7. The TEM image reveals that powders are formed by particles ranging from 30–100 nm. This is in agreement with the crystallite size of Mg-FA powders calculated using XRD data.

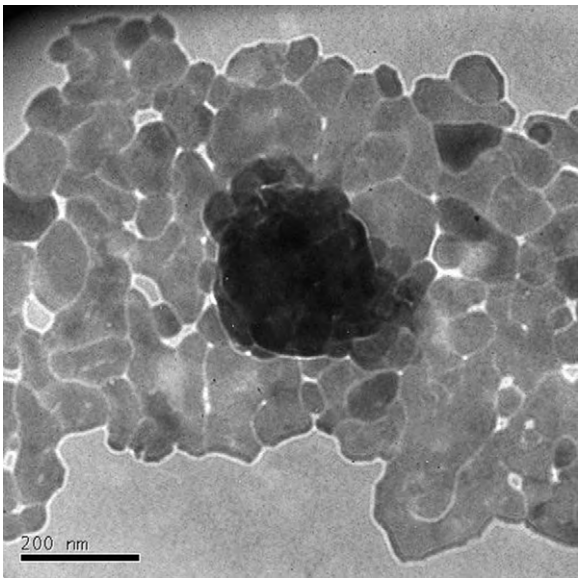

Fig. 7. TEM micrograph of FA5M powder.

Bioceramics with a grain size lower than 100 nm have superior mechanical and biological properties. It has also been showed that the dissolution rate of the bioceramic nanopowder is higher than that of conventional powder, and thus apatite is formed more easily [31,32]. The obtained powders had a crystallite size in the range of nano scale. Nanometer size characteristic for obtained powders renders them similar to natural bone. In addition, the Mg-FA materials are expected to have better biocompatibility and biological properties than pure FA.

4. Conclusions

Mg-doped fluorapatite (FA) nano powders with different Mg content were fabricated by sol–gel method. FTIR result combined with the X-ray diffraction indicated that substitution of Ca^{2+} with Mg ions in the fluorapatite matrix was successfully occurred.

The incorporation of Mg ions into the fluorapatite led to the decrease in the lattice parameters. Our results indicate that just partial amount of Mg entered into the FA lattice and the remainder formed MgF_2. The obtained powders had crystallite size of about 30–100 nm. The Mg-FA materials are expected to have better biocompatibility and biological properties than pure FA. Future

experiments should be conducted on Mg-FA to determine its bioactivity and biocompatibility.

Acknowledgement

The authors are grateful to Isfahan University of Technology for supporting the present research.

References

[1] J. Park, J. Alloys Compd. 492 (2010) L57–L60.
[2] M. Mazaheri, M. Haghighatzadeh, A.M. Zahedi, S.K. Sadrnezhaad, J. Alloys Compd. 471 (2009) 180–184.
[3] H. Arami, M. Mohajerani, M. Mazloumi, R. Khalifehzadeh, A. Lak, S.K. Sadrnezhaad, J. Alloys Compd. 469 (2009) 391–394.
[4] M. Descamps, J.C. Hornez, A. Leriche, J. Eur. Ceram. Soc. 29 (2009) 369–375.
[5] Y. Chen, X. Miao, Ceram. Int. 30 (2004) 1961–1965.
[6] J. Wang, Y. Chao, Q. Wan, Z. Zhu, H. Yu, Acta Biomater. 5 (2009) 1798–1807.
[7] N.Y. Mostafa, H.M. Hassan, F.H. Mohamed, J. Alloys Compd. 479 (2009) 692–698.
[8] A. Bianco, I. Cacciotti, M. Lombardi, L. Montanaro, Mater. Res. Bull. 44 (2009) 345–354.
[9] M.J. Jiao, X.X. Wang, Mater. Lett. 63 (2009) 2286–2289.
[10] K. Matsunaga, H. Murata, T. Mizoguchi, A. Nakahira, Acta Biomater. 6 (2010) 2289–2293.
[11] M. Chen, D. Jiang, D. Li, J. Zhu, G. Li, J. Xie, J. Alloys Compd. 485 (2009) 396–401.
[12] A. Bianco, I. Cacciotti, M. Lombardi, L. Montanaro, E. Bemporad, M. Sebastiani, Ceram. Int. 36 (2010) 313–322.
[13] H. Ye, X.Y. Liu, H.P. Hong, Appl. Surf. Sci. 255 (2009) 8126–8134.
[14] K.A. Bhadang, C.A. Holding, H. Thissen, K.M. McLean, J.S. Forsythe, D.R. Haynes, Acta Biomater. 6 (2010) 1575–1583.
[15] B.I. Bogdanov, P.S. Pashev, J.H. Hristov, I.G. Markovska, Ceram. Int. 35 (2009) 1651–1655.
[16] I. Cacciotti, A. Bianco, M. Lombardi, L. Montanaro, J. Eur. Ceram. Soc. 29 (2009) 2969–2978.
[17] G. Qi, S. Zhang, K.A. Khor, W. Weng, X. Zeng, C. Liu, Thin Solid Films 516 (2008) 5172–5175.
[18] H. Liang, Y.Z. Wan, F. He, Y. Huang, J.D. Xu, J.M. Li, Y.L. Wang, Z.G. Zhao, Appl. Surf. Sci. 253 (2007) 3326–3333.
[19] Y. Cai, S. Zhang, X. Zeng, Y. Wang, M. Qian, W. Weng, Thin Solid Films 517 (2009) 5347–5351.
[20] S.K. Ruan, J.G. Zhou, A.M. Zhong, J.F. Duan, X.B. Yang, M.Z. Su, J. Alloys Compd. 275–277 (1998) 72–75.
[21] X.H. Chuai, H.J. Zhang, F.Sh. Li, Sh.Z. Lu, J. Lin, Sh.B. Wang, K. Chi-Chou, J. Alloys Compd. 334 (2002) 211–218.
[22] E. Jallot, J.M. Nedelec, A.S. Grimault, E. Chassot, A. Grandjean-Laquerriere, P. Laquerriere, D. Laurent-Maquin, Colloids Surf. B: Biointerfaces 42 (2005) 205–210.
[23] B.D. Cullity, Elements of X-ray diffraction, 2nd ed., Addison-Wesley publishing, 1977, p. 284.
[24] T.J. Webster, E.A. Massa-Schlueter, J.L. Smith, E.B. Slamovich, Biomaterials 25 (2004) 2111–2121.
[25] Z. Yang, Y. Jiang, L.X. Yu, B. Wen, F. Li, S. Sun, T. Hou, J. Mater. Chem. 15 (2005) 1807–1811.
[26] M. Hidouri, K. Bouzouita, F. Kooli, I. Khattech, Mater. Chem. Phys. 80 (2003) 496–505.
[27] L.M. Rodriguez-Lorenzo, J.N. Hart, K.A. Gross, Biomaterials 24 (2003) 3777–3785.
[28] Y. Liu, W. Wang, Y. Zhan, C. Zheng, G. Wang, Mater. Lett. 56 (2002) 496–501.
[29] M. Okazaki, J. Takahashi, H. Kimura, Caries Res. 20 (1986) 324–331.
[30] S.R. Kim, J.H. Lee, Y.T. Kim, D.H. Riu, S.J. Jung, Y.J. Lee, S.C. Chung, Y.H. Kim, Biomaterials 24 (2003) 1389–1398.
[31] M. Kharaziha, M.H. Fathi, Ceram. Int. 35 (2009) 2449–2454.
[32] M.H. Fathi, M. Kharaziha, Mater. Lett. 63 (2009) 1455–1458.